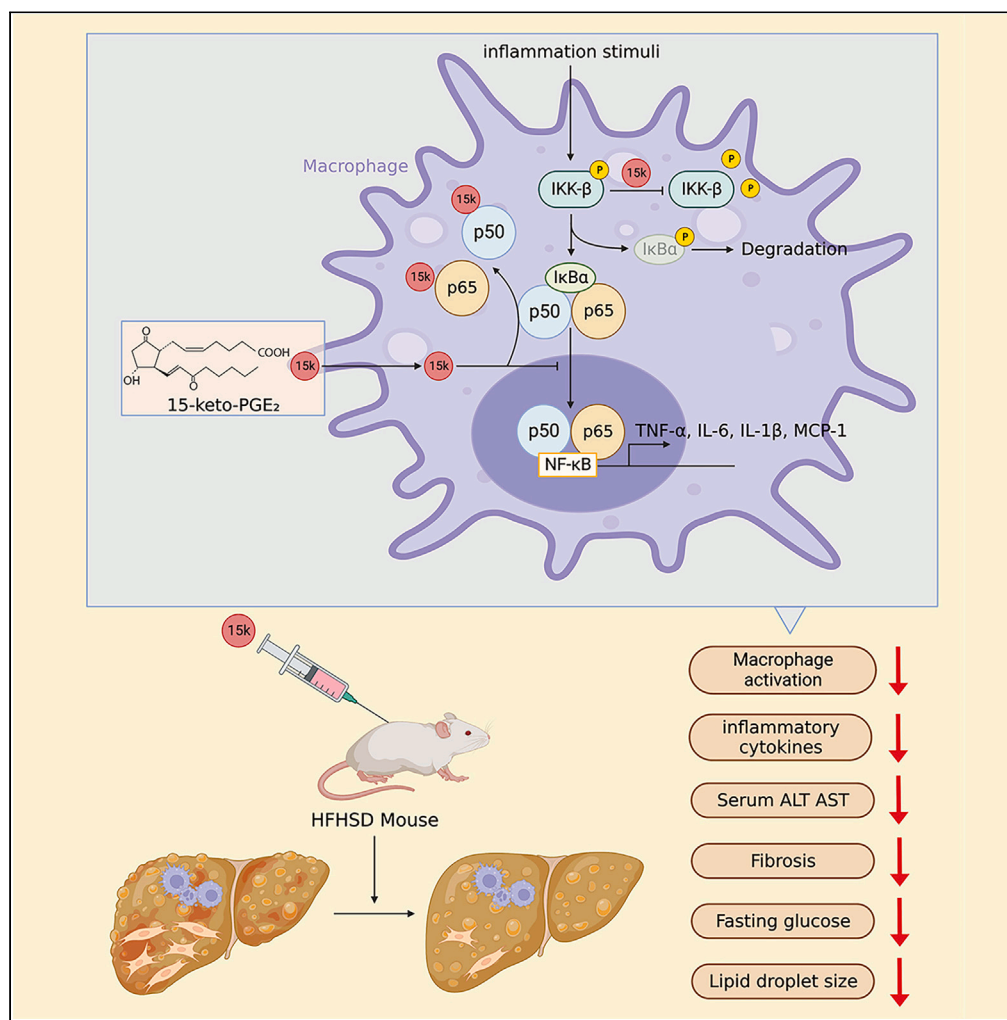


Article

15-keto-PGE₂ alleviates nonalcoholic steatohepatitis through its covalent modification of NF-κB factors



Siow-Wey Hee, Yi-Cheng Chang, Lynn Su, ..., Daniel Liao, Shiau-Mei Chen, Lee-Ming Chuang

leeming@ntu.edu.tw

Highlights

15-keto-PGE₂ inhibits NF-κB signaling in macrophages

15-keto-PGE₂ post-translationally modified NF-κB subunits

15-keto-PGE₂ reduces pro-inflammatory cytokines on a high-fat, high-sucrose diet

15-keto-PGE₂ decreases steatohepatitis in NASH mice

Hee et al., iScience 26, 107997
October 20, 2023 © 2023 The Author(s).
<https://doi.org/10.1016/j.isci.2023.107997>



Article

15-keto-PGE₂ alleviates nonalcoholic steatohepatitis through its covalent modification of NF-κB factors

Siow-Wey Hee,^{1,10} Yi-Cheng Chang,^{1,2,3,10} Lynn Su,⁴ Ing-Jung Chen,⁴ Yung-Ming Jeng,^{5,6,7} Meng-Lun Hsieh,^{1,2,9} Yu-Chia Chang,⁴ Fu-An Li,³ Daniel Liao,² Shiau-Mei Chen,¹ and Lee-Ming Chuang^{1,4,8,11,*}

SUMMARY

15-keto-PGE₂ is one of the eicosanoids with anti-inflammatory properties. In this study, we demonstrated that 15-keto-PGE₂ post-translationally modified the nuclear factor κ-light-chain-enhancer of activated B cells (NF-κB) subunits p105/p50 and p65 at Cys59 and Cys120 sites, respectively, hence inhibiting the activation of NF-κB signaling in macrophages. In mice fed a high-fat and high-sucrose diet (HFHSD), 15-keto-PGE₂ treatment reduced pro-inflammatory cytokines and fasting glucose levels. In mice with non-alcoholic steatohepatitis (NASH) induced by a prolonged HFHSD, 15-keto-PGE₂ treatment significantly decreased liver inflammation, lowered serum levels of alanine transaminase (ALT) and aspartate transferase (AST), and inhibited macrophage infiltration. It also reduced lipid droplet size and downregulated key regulators of lipogenesis. These findings highlight the potential of 15-keto-PGE₂, through NF-κB modification, in preventing the development and progression of steatohepatitis, emphasizing the significance of endogenous lipid mediators in the inflammatory response.

INTRODUCTION

Non-alcoholic fatty liver disease (NAFLD) is the primary cause of chronic liver disease, affecting around 20–30% of the general population.^{1,2} NAFLD is characterized by excessive lipid accumulation in the liver. It can progress into a more severe form of non-alcoholic steatohepatitis (NASH) characterized by a combination of steatosis, hepatocyte injury (ballooning), and hepatic inflammation, with or without fibrosis. If left untreated, NASH may eventually progress to liver cirrhosis and occasionally to hepatocellular carcinoma.^{3,4} Despite the rising global prevalence of NASH, there are currently no effective therapeutic agents.

Obesity is a high risk for developing NAFLD. Excessive consumption of a high-fat diet compels the adipocytes to uptake more lipids, which further induce macrophage infiltration, production of inflammatory cytokines and eventually adipocyte metabolic dysregulation. The increment in plasma lipid and glucose subsequently stimulates extra lipid accumulation in the liver. Disruption of the homeostasis of hepatic lipid metabolism further increases oxidative stress and hepatic insulin resistance, finally promotes hepatic injury, induces liver macrophage activation and inflammation, and driving the development of fibrosis or cirrhosis.^{5–7}

Endotoxins such as lipopolysaccharide (LPS) are potent inducers of hepatic inflammation and macrophage activation in NASH. Excessive fat and glucose intake disrupt the gut microbiome and tight junctions, increasing intestinal permeability.⁸ This allows LPS to enter the bloodstream, reaching the liver and activating Kupffer cells, the resident macrophages.^{9,10} Simultaneously, circulating monocytes are recruited to the liver, differentiate into macrophages and actively contribute to the inflammatory response. These immune cells release pro-inflammatory cytokines and molecules, promoting the accumulation of fat in the liver and exacerbating insulin resistance and impaired lipid metabolism in NASH. In particular, nuclear factor κ-light-chain-enhancer of activated B cells (NF-κB) has been implicated in mediating the inflammatory responses of activated macrophages.^{11–13}

NF-κB consists of a dimeric protein formed by the members of the Rel family of transcriptional activator proteins. It comprises mainly a heterodimer of NF-κB1 (p50) and RelA (p65). The p50 subunit is generated by proteolytic processing of a p105 precursor, whereas p65 is

¹Department of Internal Medicine, National Taiwan University Hospital, Taipei 100225, Taiwan

²Graduate Institute of Medical Genomics and Proteomics, National Taiwan University, Taipei 100225, Taiwan

³Institute of Biomedical Sciences, Academia Sinica, Taipei 115201, Taiwan

⁴Graduate Institute of Molecular Medicine, National Taiwan University, Taipei 100225, Taiwan

⁵Department of Pathology, National Taiwan University, Taipei, Taiwan

⁶Department of Pathology, National Taiwan University Hospital, Taipei, Taiwan

⁷Graduate Institute of Pathology, College of Medicine, National Taiwan University, Taipei, Taiwan

⁸Graduate Institute of Clinical Medicine, National Taiwan University, Taipei 100225, Taiwan

⁹Department of Medicinal Chemistry, University of Florida, Gainesville, FL 32610, USA

¹⁰These authors contributed equally

¹¹Lead contact

*Correspondence: leeming@ntu.edu.tw

<https://doi.org/10.1016/j.isci.2023.107997>



synthesized as a mature protein.¹⁴ In the absence of inducers, the NF- κ B heterodimer is sequestered in the cytoplasm bound to the inhibitor, I κ B α protein. Upon pro-inflammatory stimulation from pathogens and stress acting via Toll-Like receptor 4 (TLR4), I κ B α subunits become phosphorylated by the trimeric I κ B-kinase (IKK) complex, resulting in the release and translocation of NF- κ B factors to the nucleus and activation of pro-inflammatory target genes such as inducible nitric oxide synthase (iNOS), tumor necrosis factor alpha (TNF- α), interleukin-6 (IL-6), interleukin-1 β (IL-1 β), and monocyte chemoattractant protein-1 (MCP-1).^{15,16}

During the onset of inflammation, PGE₂ is one of the major lipid mediators produced.^{17,18} Upon generation, PGE₂ is catalyzed by NADH-dependent 15-hydroxyprostaglandin dehydrogenase (15-PGDH) to generate 15-keto-PGE₂.¹⁹ 15-keto-PGE₂ possesses an electrophilic carbon at the C13 position, enabling it to undergo covalent reactions with free nucleophilic residues, such as cysteine residues in cellular proteins, through the Michael addition reaction.^{20–22} Our previous studies reported that 15-keto-PGE₂ is an endogenous ligand of PPAR γ .^{23,24} We also showed that 15-keto-PGE₂ suppressed acute inflammation in a murine sepsis model through modification to Kelch-like ECH-associated protein 1 (Keap1) and activation of the Nrf2 (Nuclear factor erythroid 2-related factor 2)-related anti-oxidative pathways.²⁰ The activation of PPAR γ ²⁵ and Nrf2²⁶ pathways have been reported to ameliorate liver disease including NASH, implying that modulation of 15-keto-PGE₂ pathways may be important in preventing the progression of NAFLD/NASH disease.

In this study, we identified novel targets of 15-keto-PGE₂ and tested their anti-inflammatory effects in both cellular and mice models. We demonstrated 15-keto-PGE₂ attenuates LPS-induced macrophage activation through covalent binding to both NF- κ B subunits, p105/p50 and p65. Furthermore, administration of 15-keto-PGE₂ ameliorated both diet-induced hepatic steatosis and steatohepatitis. Our results thus suggest a novel anti-inflammatory therapy for diet-induced NASH through administering 15-keto-PGE₂.

RESULTS

15-keto-PGE₂ exhibited anti-inflammatory effects and reduced migratory ability in RAW264.7 cell model

We first examined the effect of 15-keto-PGE₂ on inflammatory responses in macrophages using the RAW264.7 cell line. LPS was chosen to treat RAW264.7 cells due to its well-established role in triggering inflammatory responses by binding to the TLR4 receptor and inducing the release of inflammatory cytokines. Compared to the untreated control cells, we observed a significant dose-dependent decrease in iNOS (Figure 1A), TNF- α (Figure 1B), IL-6 (Figure 1C), and MCP-1 (Figure 1D) levels in RAW264.7 cells treated with 15-keto-PGE₂ after LPS stimulation. Since LPS activates NF- κ B signaling in macrophages, we tested the effect of 15-keto-PGE₂ on LPS-induced phosphorylation of IKK α / β and I κ B α . Figure 1E shows that pre-treatment of 15-keto-PGE₂ specifically reduced the phosphorylation of IKK α / β but not I κ B α phosphorylation. Inactivated NF- κ B transcription factors are normally sequestered in the cytosol. Figure 1F shows a dose-dependent inhibitory effect of 15-keto-PGE₂ on the nuclear translocation of p65 and p50 upon LPS stimulation when compared with the control cells. Furthermore, 15-keto-PGE₂ treatment reduces the migration of RAW264.7 cells upon LPS induction (Figures 1G and 1H). These results suggest the inhibitory effect of NF- κ B activation is mediated through 15-keto-PGE₂.

15-keto-PGE₂ down-regulated inflammatory activity via cysteine modification on NF- κ B factors

15-keto-PGE₂ contains an electrophilic carbon at the C13 position, enabling it to form a protein adducts. Based on the observed dose-dependent reduction of pro-inflammatory responses by 15-keto-PGE₂, we hypothesized that it interacts with and modifies NF- κ B factors, p105/p50 and p65, leading to the inhibition of pro-inflammatory activity. To confirm the covalent binding of 15-keto-PGE₂ to NF- κ B factors, we generated an antibody specifically recognizing the 15-keto-PGE₂-conjugated cysteine site on the target protein. The specificity of the antibody was validated (see Figure S1). We first immunoprecipitated 15-keto-PGE₂-treated RAW264.7 lysates using an anti-p105/p50 antibody. Ten percent of the immunoprecipitated lysates were examined by SDS-PAGE to confirm the immunoprecipitation (IP) ability for p105/p50 proteins (Figure 2A), while the remaining lysates were analyzed using anti-Cys-15-keto-PGE₂ antibody. The results demonstrated that p105/p50 were covalently bound to 15-keto-PGE₂ (Figure 2B). Reciprocal IP was performed using the Cys-15-keto-PGE₂ antibody (Figure 2C), confirming the covalent modification of 15-keto-PGE₂ on p105/p50 (Figure 2D). Subsequently, we investigated the impact of 15-keto-PGE₂ treatment on the degradation of p105/p50. Cells were pre-treated with 15-keto-PGE₂, followed by LPS stimulation and cycloheximide treatment to suppress protein synthesis. Our results demonstrated that p105/p50 exhibited an accelerated degradation rate upon 15-keto-PGE₂ treatment, in both the basal state and in response to LPS, when compared to the control groups (Figure 2E). Next, we examined whether 15-keto-PGE₂ could also modify the p65 subunit in 15-keto-PGE₂-treated RAW264.7 lysates. Similarly, we subjected 10% of the anti-p65 antibody immunoprecipitated lysates to SDS-PAGE to confirm the IP capability (Figure 2F), while the remaining lysates were probed with the anti-Cys-15-keto-PGE₂ antibody. The results revealed that p65 subunits were covalently bound to 15-keto-PGE₂ (Figure 2G). Reciprocal IP using the Cys-15-keto-PGE₂ antibody further confirmed the covalent modification of 15-keto-PGE₂ on p65 (Figure 2H). Figure 2I demonstrates the dose-dependent inhibitory effect of 15-keto-PGE₂ on nuclear p65 binding to DNA sequence containing the NF- κ B response element.

15-keto-PGE₂ modified p105/p50 at Cys59 and p65 at Cys120 sites

To further determine the 15-keto-PGE₂ binding sites on p65 and p50, we transiently transfected FLAG-p65 and FLAG-p105/p50 into HEK293T cells for 24 h. We confirmed the overexpression efficiency by immunoblotting (Figure 3A) and IP (see Figure S2). The lysates immunoprecipitated with the anti-FLAG antibody were separated by SDS-PAGE and visualized using Sypro Ruby stain (Figure 3B) or Coomassie Brilliant Blue (Figure 3E). The protein bands of approximately 105 kDa, 50 kDa, and 65 kDa were excised and the tryptic peptides were further analyzed by Orbitrap mass spectrometers. We found that both p105/p50 at Cys59 (Figures 3C and 3D) and p65 at Cys120 (Figure 3F) sites were modified

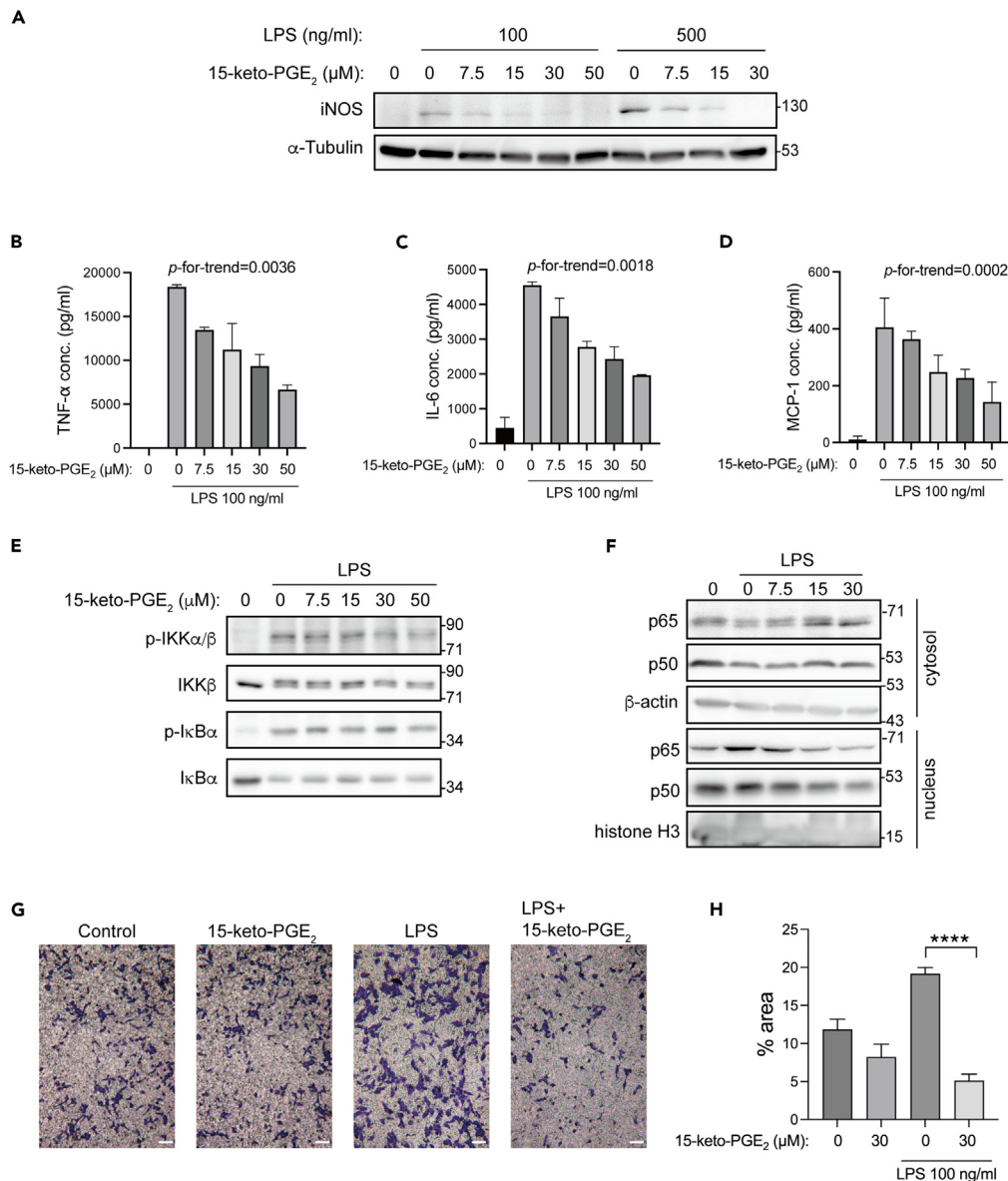


Figure 1. 15-keto-PGE₂ reduced pro-inflammatory responses in RAW264.7 cell models

(A–D) RAW264.7 cells were pre-treated with 15-keto-PGE₂ for 2 h and LPS stimulation for 16 h. The expression of iNOS (A) was determined by western blot, and the TNF-α (B), IL-6 (C), and MCP-1(D) concentrations were detected using ELISA kits.

(E) After pre-treatment with 15-keto-PGE₂ for 2 h, RAW264.7 cells were stimulated with LPS (100 ng/mL) for 15 min to determine the expression of phospho-IKK and IKK or 30 min to determine the expression of phospho-IκBα and IκBα.

(F) Nuclear-cytoplasmic fractionation was performed to evaluate the subcellular localization of p65 and p50 after LPS (100 ng/mL) stimulation for 30 min, using β-actin and histone H3 as internal control, respectively.

(G) Representative images and (H) relative quantitation showing the effects of 15-keto-PGE₂ on migration of RAW264.7 cells after treatment of LPS (1 μg/ml) for 24 h. Scale bar, 50 μm. The results shown are the mean ± SEM from a single experiment performed in triplicate, representative of two independent experiments with similar results. *P*-for-trend was used to test the linear trend. *denotes statistically significant differences: *****p* < 0.0001.

by 15-keto-PGE₂. In spectra the 15k marked in red under cysteine (C) indicates a 15-keto-PGE₂ group attached to the C, and the labels of y-series and b-series denote the detected fragment ions of the MS/MS fragmentation. Since the detected fragments are contiguous, there is high confidence in the peptide sequence and 15-keto-PGE₂ modification site.

To further confirm that 15-keto-PGE₂ could modulate the transcriptional activity of NF-κB, RAW264.7 were transfected with luciferase reporter plasmid linked to the promoters of NF-κB target genes (IgK-Luc) and treated with different concentrations of LPS (Figure 3G). Figure 3H illustrates that the 15-keto-PGE₂-treated group exhibited a significant reduction in NF-κB luciferase reporter activity at different time points

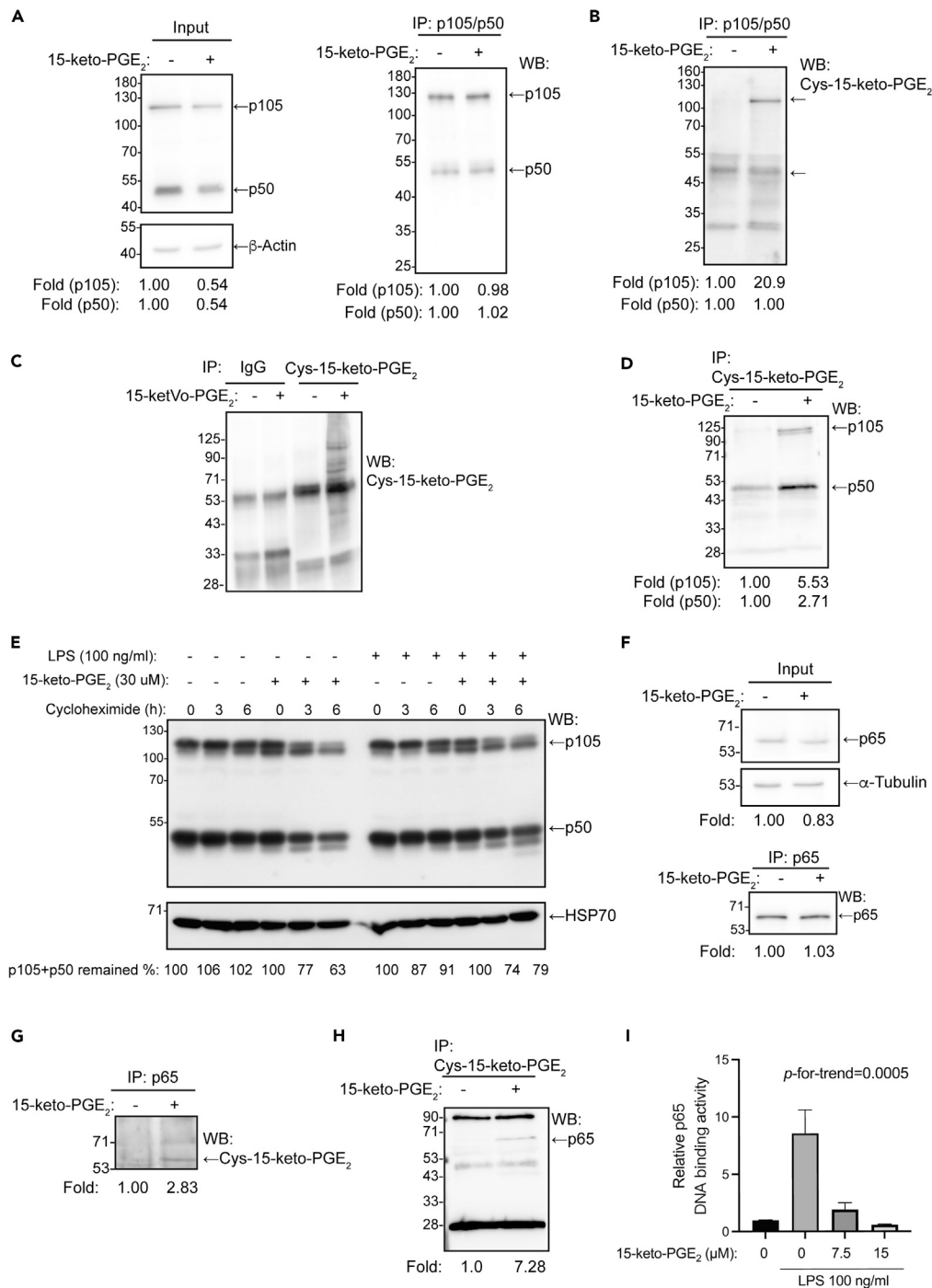


Figure 2. 15-keto-PGE₂ modulated inflammatory activity in RAW264.7 cells via cysteine modification on NF-κB

(A–H) RAW264.7 cells were pre-treated with 15-keto-PGE₂ for 2 h and stimulated with LPS for 16 h. The lysates were collected and further underwent IP using anti-p105/p50 antibody, followed by immunoblotting with anti-p105/p50 (A) and Cys-15-keto-PGE₂ (B) antibodies. Reciprocal IP was carried out using anti-Cys-15-keto-PGE₂ antibody, immunoblotted with anti-Cys-15-keto-PGE₂ (C) and anti-p105/p50 (D) antibodies, respectively. After pre-treated with 15-keto-PGE₂ for 2 h and stimulated with LPS for 16 h, cycloheximide was added for the indicated times, the protein were further separated by SDS-PAGE and visualized using anti-p105/p50 antibody. The remaining quantity of p50 + p105, which indicates degradation over time, was computed by dividing the sum of p50 + p105 measured at the indicated time point by the initial sum of p50 + p105. The result was then multiplied by 100% (E). 15-keto-PGE₂-treated RAW264.7 lysates were

Figure 2. Continued

immunoprecipitated using anti-p65 antibody and immunoblotted with p65 (F) and anti-Cys-15-keto-PGE₂ (G) antibodies. Reciprocal IP was carried out using anti-Cys-15-keto-PGE₂ antibody, immunoblotted with and anti-p65 (H) antibody.

(I) The p65 DNA binding activity was measured after 30 min of 100 ng/mL LPS-treated RAW264.7 cells with or without 2 h 15-keto-PGE₂ pre-treatment. Results were presented as fold change relative to the untreated cells. *P*-for-trend was used to test the linear trend.

following LPS stimulation. Furthermore, Figure 3I demonstrates the dose-dependent effect of the 15-keto-PGE₂-mediated inhibition on NF-κB luciferase reporter activity. We then performed site directed mutagenesis on Cys59 of p105/p50 and Cys120 of p65 to turn these residues into Alanine (p50^{C59A} and p65^{C120A}) and these plasmids were transfected into RAW264.7 cells. Compared to the cells transfected with wild type p105/p50 and p65, the inhibitory effect of 15-keto-PGE₂ on NF-κB luciferase activity in LPS-treated RAW264.7 cells was abolished in the cells transfected with p50^{C59A} and p65^{C120A}, respectively. However, the mutants also lost their function, remaining only around half of the luciferase activity (Figures 3J and 3K).

15-keto-PGE₂ reduced fasting glucose levels and inflammation in HFHSD-fed mice

Obesity is associated with chronic low-grade inflammation in adipose tissues, resulting in the production of inflammatory cytokines and increased macrophage activation. This enhanced proinflammatory signaling further contributes to systemic metabolic dysregulation.²⁷ We therefore employed a diet-induced obese mice model to validate the anti-inflammatory role of 15-keto-PGE₂. Starting from the 8th week of age, mice were fed on an HFHSD for 3 months, followed by a continual 6-day administration of 15-keto-PGE₂ (0, 3, 10, 20, and 40 mg/kg/day). Fasting glucose levels, which indicate hepatic gluconeogenesis and inversely correlate with hepatic insulin resistance, were dose-dependently lowered by 15-keto-PGE₂ treatment (Figure 4A), without affecting body weight (Figure 4B).

To observe the prolonged effect of 15-keto-PGE₂, we extended the treatment for 21 days (40 mg/kg/day). We found significantly reduced serum levels of TNF-α (Figure 4C), IL-6 (Figure 4D), IL-1β (Figure 4E), and MCP-1 (Figure 4F). Similarly, there was a trend of decreased expression of the macrophage marker F4/80 in the epididymal white adipose tissues (eWAT) (Figures 4G and 4H). Adipose tissue inflammation and macrophage infiltration are considered major contributors to systemic insulin resistance. Consistently, we observed improved glucose tolerance and insulin sensitivity with 15-keto-PGE₂ treatment (see Figure S3).

Using the Cys-15-keto-PGE₂ antibody, we found potential protein adducts of 15-keto-PGE₂ in different adipose depots after 3 days of intraperitoneal injection (Figure 4I). Furthermore, we confirmed the covalent binding of p105/p50 (Figures 4J–4L) and p65 (Figures 4M and 4N) to 15-keto-PGE₂ through direct or reciprocal IP in 15-keto-PGE₂-treated mouse adipose tissues.

Reduced nuclear localization of NF-κB protein adducts in the liver of 15-keto-PGE₂-treated HFHSD mice

High-fat induced obesity is linked with nonalcoholic fatty liver disease, ranging from simple steatosis, liver inflammation, and ultimately liver failure. We further examined the effect of the 21-day 15-keto-PGE₂ (40 mg/kg/day) treatment on liver tissues of HFHSD-fed mice. The induction of liver inflammation was mild as only a few mice showed positive staining of F4/80 macrophage marker (Figures 5A and 5B). The p65 and p50 levels in the liver nuclear extract were reduced upon 15-keto-PGE₂ administration (Figures 5C–5F). Similar to the results of adipose tissues, we found the formation of conjugated proteins in the liver of 15-keto-PGE₂-treated HFHSD mice (Figure 5G). Additionally, 15-keto-PGE₂ was shown to consistently bind to p105/p50 (Figures 5H–5J) and p65 (Figures 5K–5M) in liver tissues in either direct or reciprocal IP experiments.

15-keto-PGE₂ ameliorated hepatic steatohepatitis in long-term HFHSD-fed mice

As mentioned previously, although 3 months of HSHSD successfully induced inflammation in adipose tissues, the hepatic inflammatory response that initiates the progression of NASH is not obvious. This prompted us to prolong the HFHSD feeding period to 10 months to induce NASH. Mice were then subsequently administered 10 mg/kg/day of 15-keto-PGE₂ intraperitoneally into mice for 6 weeks. At the end of the experiment, serum alanine transaminase (ALT) (Figure 6A) and aspartate transferase (AST) (Figure 6B) were significantly decreased, and there was also a trend that both serum glucose (Figure 6C) and LPS (Figure 6D) levels were lowered after 15-keto-PGE₂ treatment. Liver tissues were collected for histopathological analyses. The H&E stain (Figure 6E) and the semi-quantitative scores of the liver revealed reversal of severe steatosis (Figure 6F), hepatocellular ballooning (Figure 6G), lobular inflammation (Figure 6H), and the NAFLD Activity Score (NAS) (Figure 6I). Furthermore, liver IHC stain also demonstrated that the treatment led to reduced activation of F4/80 macrophage marker (Figures 6J and 6K) and fibrosis marker α-smooth muscle actin (α-SMA) expression (Figures 6L and 6M).

Liver Oil Red O staining (Figure 6N) showed no change in the semi-quantitative analysis of Oil Red O-positive staining area (Figure 6O), but the lipid droplet size (Figure 6P) in 15-keto-PGE₂-treated mice was markedly reduced when compared with the vehicle control group. We next examined the expression of the major *de novo* lipogenic regulator, sterol regulatory element-binding protein-1c (Srebp-1c), and its corresponding target genes.^{28,29} As shown in Figure 6Q, treatment of 15-keto-PGE₂ significantly reduced the protein level of Srebp-1c and (Figure 6R) *Scd-1* mRNA expression. In addition, other lipogenic genes such as *Pparγ* and *Cd36* also had a tendency to decrease in the liver of 15-keto-PGE₂-treated mice (Figure 6R). All the previous results suggest that treatment with 15-keto-PGE₂ significantly ameliorates diet-induced hepatic steatohepatitis.

DISCUSSION

In this study, we evaluated the anti-inflammatory properties of 15-keto-PGE₂. Using the RAW264.7 cell model, we observed a reduction in NF-κB nuclear translocation, decreased expression of pro-inflammatory cytokines, and reduced macrophage migration. In mice subjected to an

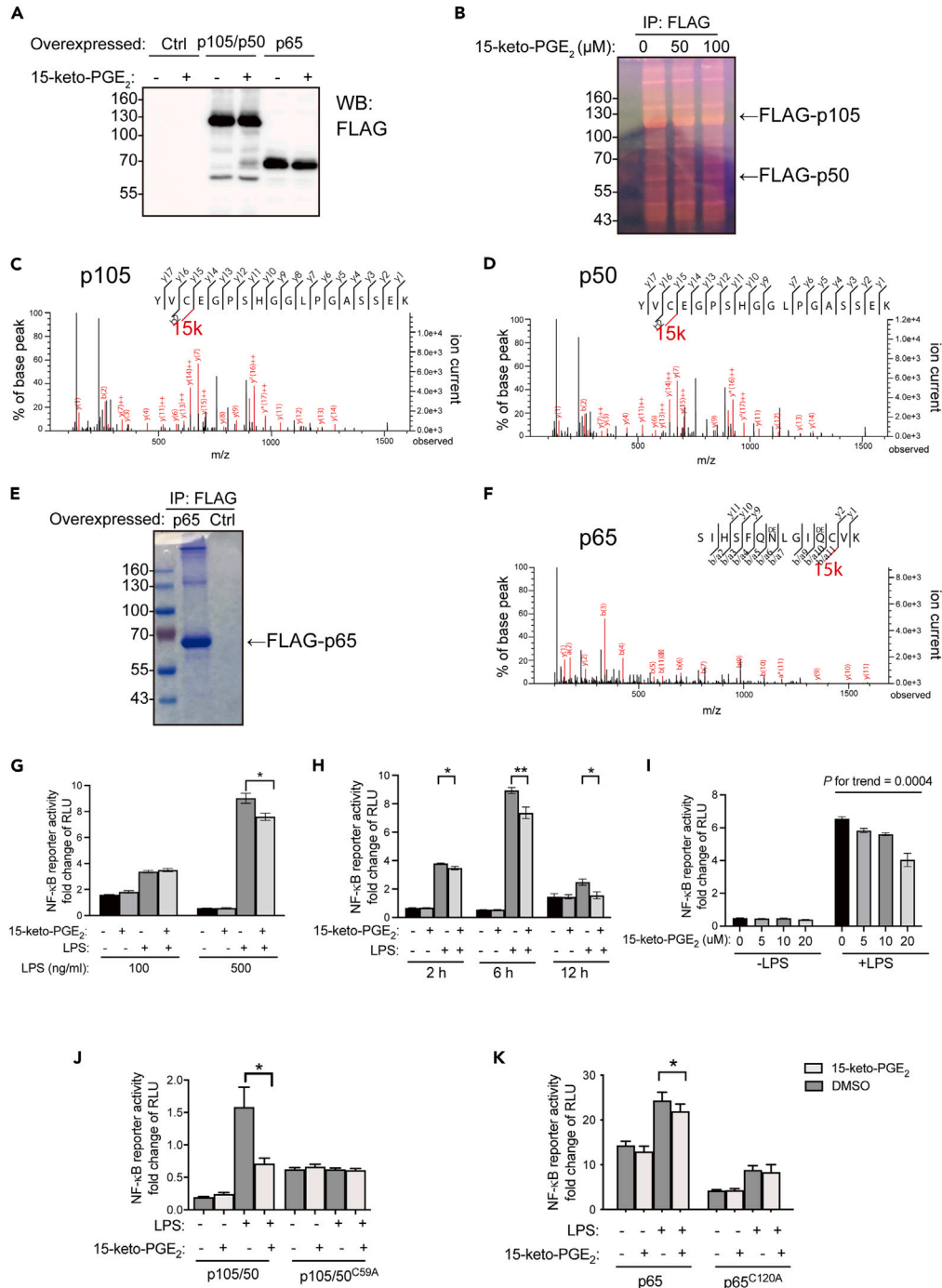


Figure 3. Identification of 15-keto-PGE₂ modification site on NF-κB components

(A) HEK293T cells were transiently transfected with FLAG-p105/p50 or FLAG-p65 for 24 h, treated with 15-keto-PGE₂ (30 μM) 24 h, and immunoblotted with anti-FLAG antibody.

(B) HEK293T cells were transfected with FLAG-p105/p50, then treated with 15-keto-PGE₂ for 24 h. FLAG-p105/p50 was then separated in SDS-PAGE for SYPRO-Ruby staining, and the gel band nearby p105 and p50 were excised for further analysis.

(C and D) Representative p105 and p50 peptide 57–74 (YCEGSPSHGGLPGASSEK) of the Cys59 site containing 15-keto-PGE₂ modification is found in 15-keto-PGE₂-treated p105 (C) and p50 (D), respectively.

(E) 15-keto-PGE₂-treated and overexpressed FLAG-p65 was separated in SDS-PAGE for Coomassie Brilliant blue staining, and bands representing p65 were excised for further analysis.

(F) Representative p65 peptide 109–122 (SIHSFQNLGIQCVK) of the Cys120 containing 15-keto-PGE₂ modification is found in 15-keto-PGE₂-treated p65.

Figure 3. Continued

(G–I) RAW264.7 cells were transfected with IgK-Luc and pRL-TK vectors. (G) They were then treated with 15-keto-PGE₂ (20 μM) with different LPS concentration, luciferase activity were measured after 6 h of treatment. (H) Time dependent (I) and dose-dependent effect of 15-keto-PGE₂ on IgK reporter activity with or without LPS (500 ng/mL) treatment.

(J and K) FLAG-p105/p50, FLAG-p105/p50^{C59A}, FLAG-p65, FLAG-p65^{C120A} were co-transfected into RAW264.7 cells with IgK-luc and pRL-TK for 24 h, and then treated with DMSO or 15-keto-PGE₂ (30 μM) for 24 h and stimulated with LPS (100 ng/mL) for 16 h. Results are expressed as fold change of RLU compared with the control groups. P-for-trend was used to test the linear trend. *p < 0.05, **p < 0.01, versus control.

HFHSD for 3 months, treatment with 15-keto-PGE₂ dose-dependently reduced fasting glucose and pro-inflammatory cytokine levels. Additionally, in mice fed the HFHSD diet for 10 months and developed steatohepatitis, 15-keto-PGE₂ treatment for 6 weeks mitigated liver injury, as shown by pathological examinations and improvements in ALT, AST, macrophage activation, and hepatic lipid droplet size. The expression of *de novo* lipogenesis genes, such as *Srebp1c* and *Scd1*, was also down-regulated.

NF-κB plays a pivotal role as a regulator of liver inflammation, and its activation is crucial in the progression of NAFLD. By using our specific generated antibody to detect the 15-keto-PGE₂-conjugated cysteine site on the target protein, we confirmed that 15-keto-PGE₂ bound to NF-κB factors p105/p50 and p65 in RAW264.7 macrophages, as well as in adipose and liver tissues treated with 15-keto-PGE₂. By using mass spectrometry analysis, we further confirmed specific modifications of 15-keto-PGE₂ at the Cys59 site of both p105 and p50. Previous studies by Toledano et al.³⁰ have demonstrated the critical role of Cys62 (the human equivalent of Cys59 in mice) as it contains a sulfhydryl group essential for DNA binding. Mutations at Cys62 can disrupt the protein surface, which interacts with DNA. Pineda-Molina et al.³¹ have also highlighted the dependence of NF-κB binding to its cognate *cis*-regulatory element on the integrity of Cys62. Moreover, this residue is surrounded by a cationic environment that renders the thiol group highly reactive and susceptible to oxidation. Additionally, our findings suggest that treatment with 15-keto-PGE₂ impacts the degradation rates of both p105 and p50 subunits, indicating the involvement of different regulated signaling pathways.

We also validated that 15-keto-PGE₂ post-translationally modified another NF-κB member, p65, at the Cys120 site, which is in the Rel homology domain (RHD), ranging from site 19 to site 187. The RHD is located near the amino-terminal region of the protein, which is responsible for its ability to recognize specific DNA sequences on the NF-κB regulated genes and form heterodimers with other NF-κB-family members.³² By affecting the RHD of p65, 15-keto-PGE₂ could inhibit the nuclear entry of p65 to reduce activation of the NF-κB pro-inflammatory pathway. It could also affect its dimerization and DNA binding ability.³³

15-keto-PGE₂ exhibits reactivity through its electrophilic carbon at the C13 position, allowing it to form covalent adducts with cellular proteins.^{21,22} This electrophilic property results from an α, β-unsaturated carbonyl group, allowing it to modify cysteine residues in various proteins and regulate their functions. In contrast, the reduced form, 13,14-dihydro-15-keto PGE₂, produced by PTGR2, lacks this electrophilic nature and doesn't exhibit similar effects.^{22,23,34} Similarly, 15-deoxy-(Delta12,14)-prostaglandin J2 (15d-PGJ2) with two α, β-unsaturated ketone moieties has shown anti-inflammatory effects by conjugating with NF-κB subunits, further supporting our findings.^{35–38} Furthermore, our study demonstrates a notable reduction in IKK phosphorylation levels upon 15-keto-PGE₂ treatment in the LPS-stimulated RAW264.7 cell model. Given IKK's pivotal role in inflammation, this modulation could have significant implications for NAFLD development.³⁹ Previously, A- and J-type cyclopentenones with varying positions of α, β-unsaturated carbonyl moieties were shown to covalently modify IKKβ at Cys179, leading to anti-inflammatory effects.⁴⁰ Although 15-keto-PGE₂ lacks a cyclopentenone structure, its α, β-unsaturated carbonyl moiety has the potential to modify IKKβ, warranting further investigation.

Recent findings underscore the importance of liver-resident and recruited macrophages in non-alcoholic steatohepatitis (NASH) and liver fibrosis progression.^{41–44} Macrophages significantly exacerbate hepatic inflammation by generating pro-inflammatory cytokines.⁴⁵ Our study employed both *in vitro* and *in vivo* models to elucidate the role of 15-keto-PGE₂ in influencing macrophage-related effects. Notably, our investigations have revealed that treatment with 15-keto-PGE₂ led to a significantly decrease in the migration of RAW264.7 macrophages. This attenuation is further supported by the reduced infiltration of F4/80 macrophages in NASH liver. Together, 15-keto-PGE₂ treatment exhibited a notable reduction in pro-inflammatory cytokine production, as evidenced in both the cellular and murine models.

To further support the role of 15-keto-PGE₂ in macrophage activation, the study conducted by Yao et al.⁴⁶ presented compelling evidence. They demonstrated that targeted overexpression of 15-PGDH, an enzyme responsible for converting PGE₂ to 15-keto-PGE₂, confers protection against LPS-induced acute liver injury *in vivo*. This protective effect was attributed to the ability of 15-keto-PGE₂ to mitigate liver inflammation induced by LPS through PPARγ activation in Kupffer cells. Additionally, our previous research showed that treatments of 15-keto-PGE₂ effectively suppress macrophage cytokine production induced by LPS by covalently modifying Keap1 at the Cys288 site and activating anti-oxidative defense mechanisms.²⁰ These findings indicate that 15-keto-PGE₂ exerts its anti-inflammatory effects by regulating various target proteins in macrophages under distinct pathophysiological conditions.

NASH is a complex and multifactorial disease. Using the Cys-15-keto-PGE₂ antibody, we identified potential targets modified by 15-keto-PGE₂ in adipose and liver tissues. Furthermore, treatment with 15-keto-PGE₂ down-regulates the expression of the lipogenic factor SREBP-1, suggesting its involvement in regulating hepatocyte lipogenesis. In a parallel study of us using an HFHSD mouse model, we observed the covalent binding of 15-keto-PGE₂ to PPARγ, accompanied by metabolic changes.³⁴ These findings provide additional evidence that 15-keto-PGE₂ exerts effects beyond macrophages and underscore its broader implications in NASH. Future studies employing global proteomic screening will uncover the cellular mechanisms associated with these potential binding proteins.

Our research has shed light on the importance of 15-keto-PGE₂ in inducing anti-inflammatory effects through the modulation of NF-κB factors in both cellular and animal models. 15-keto-PGE₂, a bioactive lipid with diverse biological effects, requires further investigation to

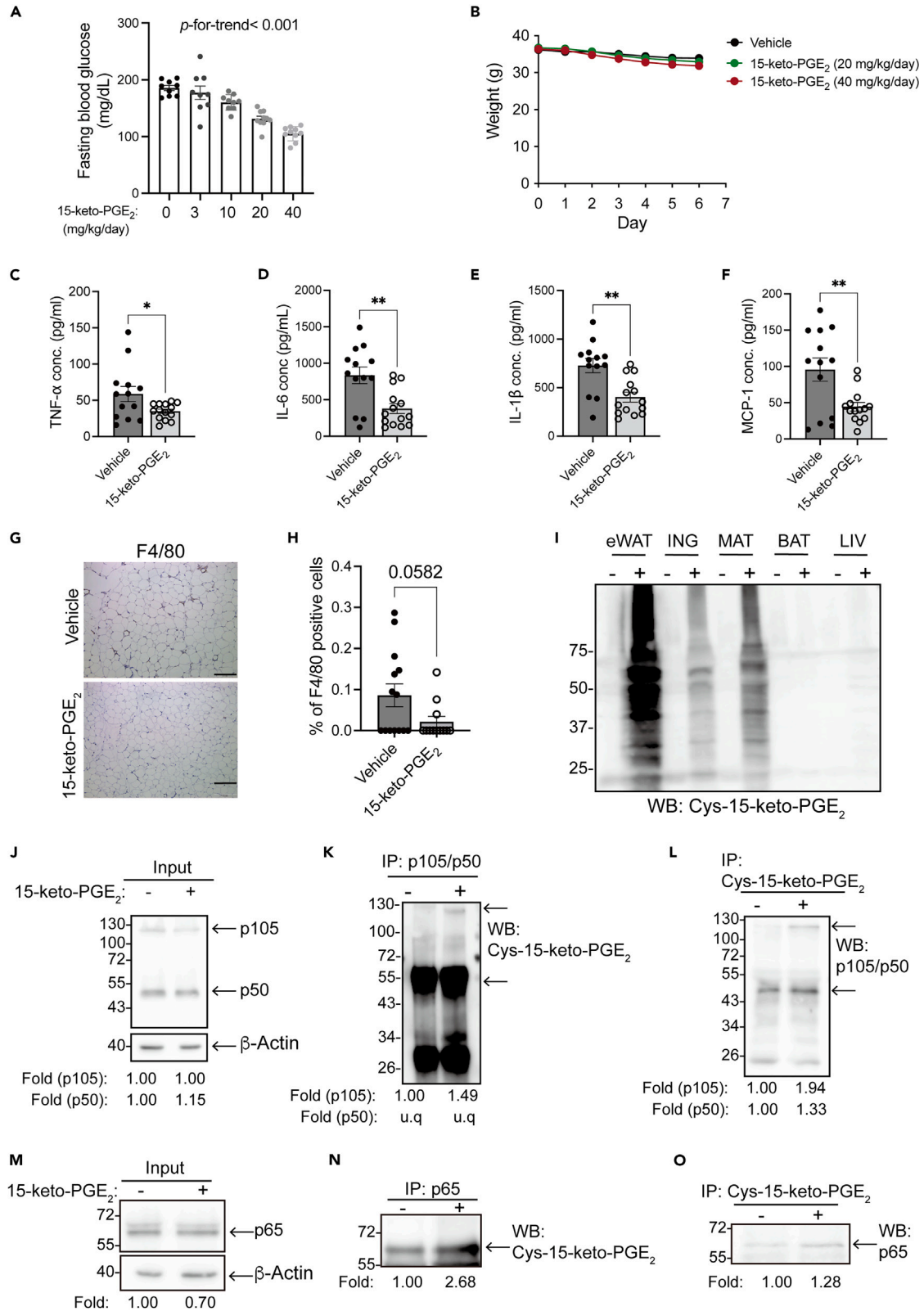


Figure 4. 15-keto-PGE reduced fasting glucose and pro-inflammatory responses in HFHSD-fed mice

(A and B) Mice fed on HFHSD for 12 weeks were intraperitoneally injected with 15-keto-PGE₂ (0, 3, 10, 20, 40 mg/kg/day) for 6 days. ((A) Changes of fasting glucose levels and (B) body weight (n = 10 per group). *P*-for-trend was used to test the linear trend.

(C–H) Plasma and epididymal fat tissues (eWAT) were harvested after administration of 15-keto-PGE₂ (40 mg/kg/day) for 21 days (n = 14–15 per group). Serum cytokine levels of TNF- α (C), IL-6 (D), IL-1 β (E), and MCP-1. (F) Immunohistochemical (IHC) stain of F4/80, scale bar, 200 μ m (G) and percentage of F4/80-positive cells in eWAT was calculated (H).

(I) eWAT, inguinal fat (ING), mesenteric fat (MAT), brown adipose fat (BAT) and liver (LIV) tissue protein lysates were subjected to SDS-PAGE and immunoblotted with anti-Cys-15-keto-PGE₂ antibody.

(J–O) The expression of p105/p50 (J) and p65 (M) were confirmed in eWAT lysates and further immunoprecipitated with anti-p105/p50 (K) or anti-p65 (N) antibodies and immunoblotted with anti-Cys-15-keto-PGE₂ antibody. Reciprocal IP was carried out using Cys-15-keto-PGE₂ antibody and immunoblotted with anti-p105/p50 (L) and anti-p65 (O) antibodies. u.q: unquantified. **p* < 0.05, ***p* < 0.01, versus control.

elucidate its specific underlying mechanisms. NASH presents a pressing medical challenge, given its rapid growth in the population and significant global burden.⁴⁷ A comprehensive understanding of 15-keto-PGE₂ would greatly facilitate the development of novel therapeutic approaches.

Limitations of the study

Our study has certain limitations. Firstly, in our RAW264.7 cellular model, we were unable to validate the impact of mutated sites in p105/p50 and p65 because the transfected mutants exhibited reduced functionality compared to the wild-type subunits. This demonstrates the importance of the specific mutated sites for the normal function of p105/p50-C59A and p65-C120A. Additionally, delivering the NF- κ B plasmids into RAW264.7 cells, which express a high level of wild-type NF- κ B subunits, may diminish the significant differences in NF- κ B reporter activity results.

Furthermore, in the long-term 10-month HFHSD-induced NASH mice model, we observed promising effects of 15-keto-PGE₂ in reducing inflammation. However, due to the small sample size (n = 4 per group), many tested parameters only reached marginal statistical significance. Additionally, although we noticed a decrease in lipogenic gene expression and lipid droplet size, the administration of 15-keto-PGE₂ did not result in significant changes in serum triglyceride (TG) and total cholesterol (T-Cho) levels, nor hepatic TG and T-Cho content. Lastly, further investigation is required to validate a recent hypothesis suggesting that 15-keto-PGE₂ may function as a weak agonist of the prostanoid receptor EP2, which terminates the inflammatory response induced by PGE₂ through the EP4 receptor.⁴⁸

STAR★METHODS

Detailed methods are provided in the online version of this paper and include the following:

- KEY RESOURCES TABLE
- RESOURCE AVAILABILITY
 - Lead contact
 - Materials availability
 - Data and code availability
- EXPERIMENTAL MODEL AND SUBJECT DETAILS
 - Mouse model of obesity and the formulation of 15-keto-PGE₂ for injection
- METHOD DETAILS
 - Cell culture and reagents
 - RNA Extraction and quantitative PCR
 - Western Blot analysis
 - Generation of monoclonal antibodies against 15-keto-PGE₂ conjugated to cysteine
 - Nuclear-cytoplasmic fractionation
 - Transwell migration assay
 - NF- κ B p65 transcription factor assays
 - Luciferase reporter assay
 - Plasmid mutagenesis
 - Immunoprecipitation and proteomic analysis
 - Measurement of metabolic parameters
 - Immunohistochemical (IHC) staining
 - Liver histopathology
 - Oil Red O staining
- QUANTIFICATION AND STATISTICAL ANALYSIS

SUPPLEMENTAL INFORMATION

Supplemental information can be found online at <https://doi.org/10.1016/j.isci.2023.107997>.

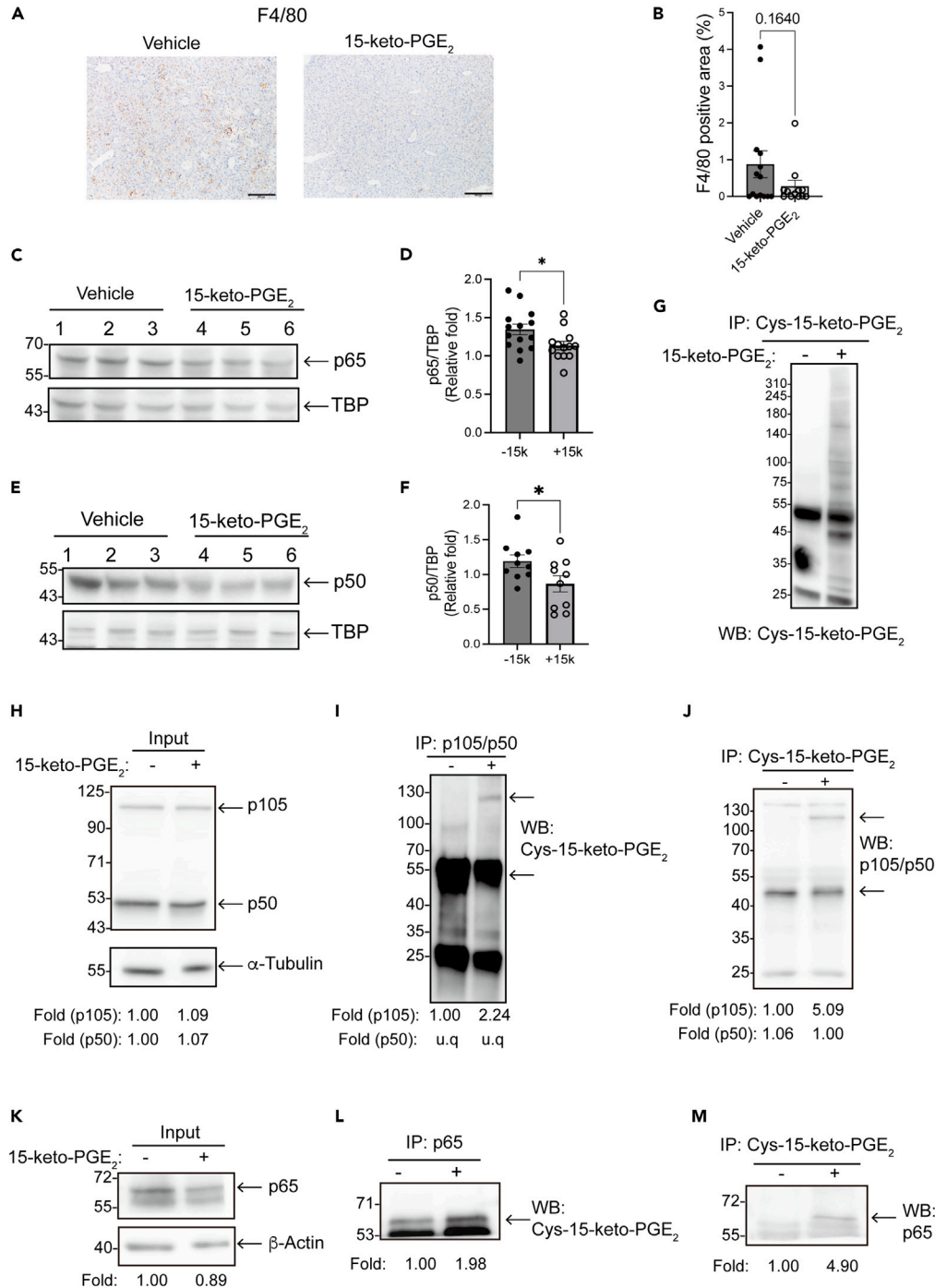


Figure 5. Formation of 15-keto-PGE₂-conjugated proteins in liver tissues of HFHSD mice

(A–F) Mice fed on HFHSD for 12 weeks were intraperitoneally injected with vehicle or 15-keto-PGE₂ (40 mg/kg/day) for 21 days and liver tissues were harvested (n = 10–15 per group) (A) IHC stain of F4/80, scale bar, 200 μm and (B) the percentage of F4/80-positive cells were calculated. Representative immunoblots of liver nuclear fraction protein of NF-κB p65 (C) and p50 (E), using TBP as loading control. Relative quantitative expression of p65 (D) and p50 (F) were calculated using ImageJ.

(G–M) Liver protein lysates were immunoprecipitated and immunoblotted with anti-Cys-15-keto-PGE₂ antibody. The expression of p105/p50 (H) and p65 (K) were confirmed in liver lysates. Liver lysates were immunoprecipitated with anti-p105/p50 (I) or anti-p65 (L) antibodies and immunoblotted with anti-Cys-15-keto-PGE₂ antibody. Reciprocal IP was carried out using anti-Cys-15-keto-PGE₂ antibody, immunoblotted with anti-p105/p50 (J) and anti-p65 (M) antibodies, respectively. u.q: unquantified. *p < 0.05, versus control.

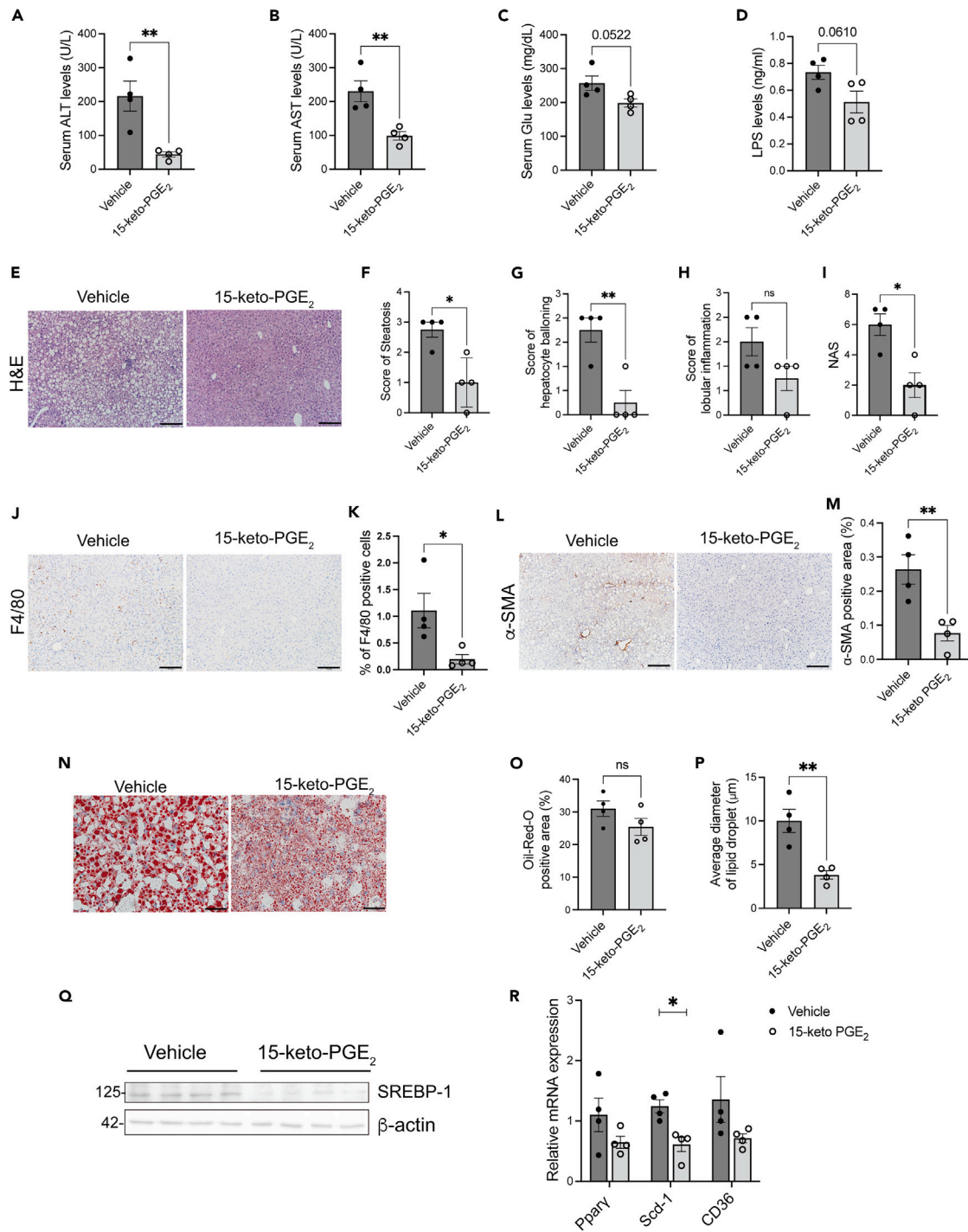


Figure 6. 15-keto-PGE₂ improves HFHSD-induced steatohepatitis in mice

(A–R) After HFHSD feeding for 10 months, mice were treated with vehicle or 15-keto-PGE₂ (10 mg/kg/day) for 6 weeks. At the end of the experiment, plasma and liver tissues were harvested for analysis of NASH (n = 4 per group). Serum levels of (A) ALT, (B) AST, (C) glucose, and (D) LPS were measured. (E) H&E stain of the liver, scale bar, 200 μm. The score of steatosis (F), hepatocyte ballooning (G), lobular inflammation (H), and NAS (I) were determined. IHC stain of F4/80, scale bar, 200 μm (J) and percentage of F4/80-positive cells of the liver were calculated (K). The IHC stain of α-SMA, scale bar, 200 μm (L) and percentage of α-SMA-positive cells of the liver were calculated (M). Liver Oil Red O staining, scale bar, 50 μm (N), percentage of Oil Red O staining area (O), and the average diameter of lipid droplets (P) were quantified. (Q) Liver protein was collected, and SREBP-1 was analyzed by immunoblotting, using β-actin as an internal control. (R) Relative mRNA expression levels of *Pparγ*, *Scd-1*, and *CD36* in the liver were measured using qRT-PCR analysis. mRNA expression levels were presented as values relative to the vehicle-treated group. ns: not significant. *p < 0.05, **p < 0.01, versus control.

ACKNOWLEDGMENTS

We thank Dr. Chia-Li Yu's lab, Institute of Molecular Medicine, National Taiwan University College of Medicine, Taipei, Taiwan, for providing us with RAW264.7 cells. We thank Dr. Li-Chung Hsu's lab, Institute of Molecular Medicine, National Taiwan University College of Medicine, Taipei, Taiwan, for providing us with IgK-luc plasmid. We thank the Metabolomics Core Facility, Scientific Instrument Center, and Proteomics Core Facility, Institute of Biomedical Sciences, Academia Sinica, for providing mass spectrometry analysis services. LTQ-Orbitrap data and additional technical assistance were provided by the Common Mass Spectrometry Facilities located at the Institute of Biological Chemistry, Academia Sinica. This work was supported by the Ministry of Science and Technology (109-2314-B-002-195-MY3).

AUTHOR CONTRIBUTIONS

L.M.C., Y.C.C., S.W.H. conceived and supervised the project. S.W.H., Y.C.C., L.S. conducted most of the experiments and analyzed the data. M.L.H., Y.C.C., Y.M.J., F.A.L. conducted some of the experiments. S.W.H., L.S. analyzed data and wrote the manuscript. D.L. drew the graphical abstract, I.J.C., S.M.C. provided opinions and ideas for reference. All the authors have reviewed and approved the final version of the manuscript.

DECLARATION OF INTERESTS

All authors declared no competing financial interests.

DECLARATION OF GENERATIVE AI AND AI-ASSISTED TECHNOLOGIES IN THE WRITING PROCESS

During the preparation of this work the author used ChatGPT in order to improve language and readability. After using this tool/service, the authors reviewed and edited the content as needed and take full responsibility for the content of the publication.

Received: February 18, 2023

Revised: August 11, 2023

Accepted: September 18, 2023

Published: September 22, 2023

REFERENCES

- Carr, R.M., Oranu, A., and Khungar, V. (2016). Nonalcoholic Fatty Liver Disease: Pathophysiology and Management. *Gastroenterol. Clin. N. Am.* *45*, 639–652. <https://doi.org/10.1016/j.gtc.2016.07.003>.
- Fazel, Y., Koenig, A.B., Sayiner, M., Goodman, Z.D., and Younossi, Z.M. (2016). Epidemiology and natural history of non-alcoholic fatty liver disease. *Metabolism* *65*, 1017–1025. <https://doi.org/10.1016/j.metabol.2016.01.012>.
- Chen, Z., Yu, R., Xiong, Y., Du, F., and Zhu, S. (2017). A vicious circle between insulin resistance and inflammation in nonalcoholic fatty liver disease. *Lipids Health Dis.* *16*, 203. <https://doi.org/10.1186/s12944-017-0572-9>.
- Kim, H., Lee, D.S., An, T.H., Park, H.J., Kim, W.K., Bae, K.H., and Oh, K.J. (2021). Metabolic Spectrum of Liver Failure in Type 2 Diabetes and Obesity: From NAFLD to NASH to HCC. *Int. J. Mol. Sci.* *22*, 4495. <https://doi.org/10.3390/ijms22094495>.
- Polyzos, S.A., Kountouras, J., and Mantzoros, C.S. (2019). Obesity and nonalcoholic fatty liver disease: From pathophysiology to therapeutics. *Metabolism* *92*, 82–97. <https://doi.org/10.1016/j.metabol.2018.11.014>.
- Divella, R., Mazzocca, A., Daniele, A., Sabbà, C., and Paradiso, A. (2019). Obesity, Nonalcoholic Fatty Liver Disease and Adipocytokines Network in Promotion of Cancer. *Int. J. Biol. Sci.* *15*, 610–616. <https://doi.org/10.7150/ijbs.29599>.
- Arab, J.P., Arrese, M., and Trauner, M. (2018). Recent Insights into the Pathogenesis of Nonalcoholic Fatty Liver Disease. *Annu. Rev. Pathol.* *13*, 321–350. <https://doi.org/10.1146/annurev-pathol-020117-043617>.
- Kessoku, T., Kobayashi, T., Imajo, K., Tanaka, K., Yamamoto, A., Takahashi, K., Kasai, Y., Ozaki, A., Iwaki, M., Nogami, A., et al. (2021). Endotoxins and Non-Alcoholic Fatty Liver Disease. *Front. Endocrinol.* *12*, 770986. <https://doi.org/10.3389/fendo.2021.770986>.
- Zhan, Y.T., and An, W. (2010). Roles of liver innate immune cells in nonalcoholic fatty liver disease. *World J. Gastroenterol.* *16*, 4652–4660. <https://doi.org/10.3748/wjg.v16.i37.4652>.
- Soares, J.B., Pimentel-Nunes, P., Roncon-Albuquerque, R., and Leite-Moreira, A. (2010). The role of lipopolysaccharide/toll-like receptor 4 signaling in chronic liver diseases. *Hepatol. Int.* *4*, 659–672. <https://doi.org/10.1007/s12072-010-9219-x>.
- Kolios, G., Valatas, V., and Kouroumalis, E. (2006). Role of Kupffer cells in the pathogenesis of liver disease. *World J. Gastroenterol.* *12*, 7413–7420. <https://doi.org/10.3748/wjg.v12.i46.7413>.
- Duarte, N., Coelho, I.C., Patarrão, R.S., Almeida, J.I., Penha-Gonçalves, C., and Macedo, M.P. (2015). How Inflammation Impinges on NAFLD: A Role for Kupffer Cells. *BioMed Res. Int.* *2015*, 984578. <https://doi.org/10.1155/2015/984578>.
- Cai, D., Yuan, M., Frantz, D.F., Melendez, P.A., Hansen, L., Lee, J., and Shoelson, S.E. (2005). Local and systemic insulin resistance resulting from hepatic activation of IKK-beta and NF-kappaB. *Nat. Med.* *11*, 183–190. <https://doi.org/10.1038/nm1166>.
- Sears, C., Olesen, J., Rubin, D., Finley, D., and Maniatis, T. (1998). NF-kappa B p105 processing via the ubiquitin-proteasome pathway. *J. Biol. Chem.* *273*, 1409–1419. <https://doi.org/10.1074/jbc.273.3.1409>.
- Rahman, M.M., and McFadden, G. (2011). Modulation of NF-kappaB signalling by microbial pathogens. *Nat. Rev. Microbiol.* *9*, 291–306. <https://doi.org/10.1038/nrmicro2539>.
- Lawrence, T. (2009). The nuclear factor NF-kappaB pathway in inflammation. *Cold Spring Harbor Perspect. Biol.* *1*, a001651. <https://doi.org/10.1101/cshperspect.a001651>.
- Tsuge, K., Inazumi, T., Shimamoto, A., and Sugimoto, Y. (2019). Molecular mechanisms underlying prostaglandin E2-exacerbated inflammation and immune diseases. *Int. Immunol.* *31*, 597–606. <https://doi.org/10.1093/intimm/dxz021>.
- Nakanishi, M., and Rosenberg, D.W. (2013). Multifaceted roles of PGE2 in inflammation and cancer. *Semin. Immunopathol.* *35*, 123–137. <https://doi.org/10.1007/s00281-012-0342-8>.
- Tai, H.H., Ensor, C.M., Tong, M., Zhou, H., and Yan, F. (2002). Prostaglandin catabolizing enzymes. *Prostag. Other Lipid Mediat.* *68–69*, 483–493. [https://doi.org/10.1016/s0090-6980\(02\)00050-3](https://doi.org/10.1016/s0090-6980(02)00050-3).
- Chen, I.J., Hee, S.W., Liao, C.H., Lin, S.Y., Su, L., Shun, C.T., and Chuang, L.M. (2018). Targeting the 15-keto-PGE2-PTGR2 axis modulates systemic inflammation and survival in experimental sepsis. *Free Radic. Biol. Med.* *115*, 113–126. <https://doi.org/10.1016/j.freeradbiomed.2017.11.016>.
- Shiraki, T., Kamiya, N., Shiki, S., Kodama, T.S., Kakizuka, A., and Jingami, H. (2005). Alpha,beta-unsaturated ketone is a core

- moiety of natural ligands for covalent binding to peroxisome proliferator-activated receptor gamma. *J. Biol. Chem.* 280, 14145–14153. <https://doi.org/10.1074/jbc.M500901200>.
22. Lee, E.J., Kim, S.J., Hahn, Y.I., Yoon, H.J., Han, B., Kim, K., Lee, S., Kim, K.P., Suh, Y.G., Na, H.K., and Surh, Y.J. (2019). 15-Keto prostaglandin E(2) suppresses STAT3 signaling and inhibits breast cancer cell growth and progression. *Redox Biol.* 23, 101175. <https://doi.org/10.1016/j.redox.2019.101175>.
 23. Chou, W.L., Chuang, L.M., Chou, C.C., Wang, A.H.J., Lawson, J.A., FitzGerald, G.A., and Chang, Z.F. (2007). Identification of a novel prostaglandin reductase reveals the involvement of prostaglandin E2 catabolism in regulation of peroxisome proliferator-activated receptor gamma activation. *J. Biol. Chem.* 282, 18162–18172. <https://doi.org/10.1074/jbc.M702289200>.
 24. Yu, Y.H., Chang, Y.C., Su, T.H., Nong, J.Y., Li, C.C., and Chuang, L.M. (2013). Prostaglandin reductase-3 negatively modulates adipogenesis through regulation of PPARgamma activity. *J. Lipid Res.* 54, 2391–2399. <https://doi.org/10.1194/jlr.M037556>.
 25. Skat-Rørdam, J., Højland Ipsen, D., Lykkesfeldt, J., and Tveden-Nyborg, P. (2019). A role of peroxisome proliferator-activated receptor gamma in non-alcoholic fatty liver disease. *Basic Clin. Pharmacol. Toxicol.* 124, 528–537. <https://doi.org/10.1111/bcpt.13190>.
 26. Xu, L., Nagata, N., and Ota, T. (2019). Impact of Glucoraphanin-Mediated Activation of Nrf2 on Non-Alcoholic Fatty Liver Disease with a Focus on Mitochondrial Dysfunction. *Int. J. Mol. Sci.* 20, 5920. <https://doi.org/10.3390/ijms20235920>.
 27. Sell, H., Habich, C., and Eckel, J. (2012). Adaptive immunity in obesity and insulin resistance. *Nat. Rev. Endocrinol.* 8, 709–716. <https://doi.org/10.1038/nrendo.2012.114>.
 28. Shimomura, I., Matsuda, M., Hammer, R.E., Bashmakov, Y., Brown, M.S., and Goldstein, J.L. (2000). Decreased IRS-2 and increased SREBP-1c lead to mixed insulin resistance and sensitivity in livers of lipodystrophic and ob/ob mice. *Mol. Cell* 6, 77–86.
 29. Ferré, P., and Foufelle, F. (2010). Hepatic steatosis: a role for *de novo* lipogenesis and the transcription factor SREBP-1c. *Diabetes Obes. Metabol.* 12, 83–92. <https://doi.org/10.1111/j.1463-1326.2010.01275.x>.
 30. Toledano, M.B., Ghosh, D., Trinh, F., and Leonard, W.J. (1993). N-terminal DNA-binding domains contribute to differential DNA-binding specificities of NF-kappa B p50 and p65. *Mol. Cell Biol.* 13, 852–860. <https://doi.org/10.1128/mcb.13.2.852-860.1993>.
 31. Pineda-Molina, E., Klatt, P., Vázquez, J., Marina, A., García de Lacoba, M., Pérez-Sala, D., and Lamas, S. (2001). Glutathionylation of the p50 subunit of NF-kappaB: a mechanism for redox-induced inhibition of DNA binding. *Biochemistry* 40, 14134–14142. <https://doi.org/10.1021/bi011459o>.
 32. Lecoq, L., Raiola, L., Chabot, P.R., Cyr, N., Arseneault, G., Legault, P., and Omichinski, J.G. (2017). Structural characterization of interactions between transactivation domain 1 of the p65 subunit of NF-kappaB and transcription regulatory factors. *Nucleic Acids Res.* 45, 5564–5576. <https://doi.org/10.1093/nar/gkx146>.
 33. Hayden, M.S., and Ghosh, S. (2008). Shared principles in NF-kappaB signaling. *Cell* 132, 344–362. <https://doi.org/10.1016/j.cell.2008.01.020>.
 34. Tseng, Y., Chuang, L., Chang, Y., Hsieh, M., Tsou, L., Chen, S., Ke, Y., Hung, M., Hee, S., Lee, H., et al. Increasing endogenous PPARγ ligands improves insulin sensitivity and protects against diet-induced obesity without side effects of thiazolidinediones. <https://assets.researchsquare.com/files/rs-490889/v1/33de9c29-1745-46c5-af04-ab64678a28e4.pdf?c=1631882793>.
 35. Kim, E.H., and Surh, Y.J. (2006). 15-Deoxy-Delta12,14-prostaglandin J2 as a potential endogenous regulator of redox-sensitive transcription factors. *Biochem. Pharmacol.* 72, 1516–1528. <https://doi.org/10.1016/j.bcp.2006.07.030>.
 36. Pérez-Sala, D. (2011). Electrophilic eicosanoids: Signaling and targets. *Chem. Biol. Interact.* 192, 96–100. <https://doi.org/10.1016/j.cbi.2010.10.003>.
 37. Straus, D.S., Pascual, G., Li, M., Welch, J.S., Ricote, M., Hsiang, C.H., Sengchanthalangsy, L.L., Ghosh, G., and Glass, C.K. (2000). 15-Deoxy-delta 12,14-prostaglandin J2 inhibits multiple steps in the NF-kappa B signaling pathway. *Proc. Natl. Acad. Sci. USA* 97, 4844–4849. <https://doi.org/10.1073/pnas.97.9.4844>.
 38. Cernuda-Morollón, E., Pineda-Molina, E., Cañada, F.J., and Pérez-Sala, D. (2001). 15-Deoxy-Delta 12,14-prostaglandin J2 inhibition of NF-kappaB-DNA binding through covalent modification of the p50 subunit. *J. Biol. Chem.* 276, 35530–35536. <https://doi.org/10.1074/jbc.M104518200>.
 39. Huh, J.Y., and Saltiel, A.R. (2021). Roles of IkkappaB kinases and TANK-binding kinase 1 in hepatic lipid metabolism and nonalcoholic fatty liver disease. *Exp. Mol. Med.* 53, 1697–1705. <https://doi.org/10.1038/s12276-021-00712-w>.
 40. Rossi, A., Kapahi, P., Natoli, G., Takahashi, T., Chen, Y., Karin, M., and Santoro, M.G. (2000). Anti-inflammatory cyclopentenone prostaglandins are direct inhibitors of IkkappaB kinase. *Nature* 403, 103–108. <https://doi.org/10.1038/47520>.
 41. Baffy, G. (2009). Kupffer cells in non-alcoholic fatty liver disease: the emerging view. *J. Hepatol.* 51, 212–223. <https://doi.org/10.1016/j.jhep.2009.03.008>.
 42. Tosello-Tramont, A.C., Landes, S.G., Nguyen, V., Novobrantseva, T.I., and Hahn, Y.S. (2012). Kupffer cells trigger nonalcoholic steatohepatitis development in diet-induced mouse model through tumor necrosis factor-alpha production. *J. Biol. Chem.* 287, 40161–40172. <https://doi.org/10.1074/jbc.M112.417014>.
 43. Rivera, C.A., Adegboyega, P., van Rooijen, N., Tagalicud, A., Allman, M., and Wallace, M. (2007). Toll-like receptor-4 signaling and Kupffer cells play pivotal roles in the pathogenesis of non-alcoholic steatohepatitis. *J. Hepatol.* 47, 571–579. <https://doi.org/10.1016/j.jhep.2007.04.019>.
 44. Park, S.J., Garcia Diaz, J., Um, E., and Hahn, Y.S. (2023). Major roles of kupffer cells and macrophages in NAFLD development. *Front. Endocrinol.* 14, 1150118. <https://doi.org/10.3389/fendo.2023.1150118>.
 45. Kazankov, K., Jørgensen, S.M.D., Thomsen, K.L., Møller, H.J., Vilstrup, H., George, J., Schuppan, D., and Grønbaek, H. (2019). The role of macrophages in nonalcoholic fatty liver disease and nonalcoholic steatohepatitis. *Nat. Rev. Gastroenterol. Hepatol.* 16, 145–159. <https://doi.org/10.1038/s41575-018-0082-x>.
 46. Yao, L., Chen, W., Song, K., Han, C., Gandhi, C.R., Lim, K., and Wu, T. (2017). 15-hydroxyprostaglandin dehydrogenase (15-PGDH) prevents lipopolysaccharide (LPS)-induced acute liver injury. *PLoS One* 12, e0176106. <https://doi.org/10.1371/journal.pone.0176106>.
 47. Vuppalaanchi, R., Nouredin, M., Alkhoury, N., and Sanyal, A.J. (2021). Therapeutic pipeline in nonalcoholic steatohepatitis. *Nat. Rev. Gastroenterol. Hepatol.* 18, 373–392. <https://doi.org/10.1038/s41575-020-00408-y>.
 48. Endo, S., Suganami, A., Fukushima, K., Senoo, K., Araki, Y., Regan, J.W., Mashimo, M., Tamura, Y., and Fujino, H. (2020). 15-Keto-PGE(2) acts as a biased/partial agonist to terminate PGE(2)-evoked signaling. *J. Biol. Chem.* 295, 13338–13352. <https://doi.org/10.1074/jbc.RA120.013988>.
 49. Lee, C.H., Lou, Y.C., and Wang, A.H.J. (2021). DMTMM-Mediated Intramolecular Cyclization of Acidic Residues in Peptides/Proteins. *ACS Omega* 6, 4708–4718. <https://doi.org/10.1021/acsomega.0c05503>.
 50. Kleiner, D.E., Brunt, E.M., Van Natta, M., Behling, C., Contos, M.J., Cummings, O.W., Ferrell, L.D., Liu, Y.C., Torbenson, M.S., Unalp-Arida, A., et al. (2005). Design and validation of a histological scoring system for nonalcoholic fatty liver disease. *Hepatology* 41, 1313–1321. <https://doi.org/10.1002/hep.20701>.

STAR★METHODS

KEY RESOURCES TABLE

REAGENT or RESOURCE	SOURCE	IDENTIFIER
Antibodies		
NF- κ B1 (p105/p50)	Cell Signaling Technologies, MA	Cat# 13586; RRID:AB_2665516
Phospho-IKK α / β (Ser176/180)	Cell Signaling Technologies, MA	Cat#2697; RRID:AB_2079382
IKK β	Cell Signaling Technologies, MA	Cat#8943; RRID:AB_11024092
Phospho-I κ B α (Ser32)	Cell Signaling Technologies, MA	Cat#2859; RRID:AB_561111
I κ B α	Cell Signaling Technologies, MA	Cat#4814; RRID:AB_390781
iNOS	Cell Signaling Technologies, MA	Cat# 2982; RRID:AB_1078202
NF- κ B Rel A (p65)	Genetex, CA	Cat# GTX102090; RRID:AB_10630493
SREBP1	Genetex, CA	Cat# GTX79299; RRID:AB_11168147
β -actin	Proteintech, IL	Cat#60008; RRID:AB_2223182
α -tubulin	Proteintech, IL	Cat# 66031; RRID:AB_2687491
histone H3	Abcam, UK	Cat# AB1791; RRID:AB_302613
F4/80	Abcam, UK	Cat# AB6640; RRID: AB_1140040
α -SMA	Abcam, UK	Cat# AB5694; RRID: AB_2223021
FLAG M2	Sigma-Aldrich, MO	Cat# F1804; RRID:AB_262044
Cys-15-keto-PGE ₂ , See in STAR Methods and Figure S1	This manuscript	N/A
TBP	Genetex, CA	Cat# GTX133204; RRID:AB_2886862
Chemicals, peptides, and recombinant proteins		
RPMI 1640	Corning	10-040-CV
fetal bovine serum,	Gibco, CA	10437-028
DMEM	Corning	10-013-CV
15-keto-PGE ₂	Cayman, MI	14720
Lipopolysaccharide, <i>E. coli</i> O111: B4 (LPS)	Millipore, MA	L4391
REzol C&T	PROtech technologies, Taiwan	PT-KP200CT
Maxima H minus Reverse Transcriptase	Thermo Scientific, MA	EP0752
Luminaris Color HiGreen qPCR Master Mix	Thermo Scientific	K0393
RIPA Lysis Buffer, 10X	Millipore	20-188
polyvinylidene fluoride (PVDF) microporous membrane	Millipore	IPVH85R
Luminata Crescendo Western HRP substrate	Millipore	WBLUR0500
TurboFect Transfection Reagents	Thermo Scientific	R0531
SYPRO-Ruby	Sigma-Aldrich	S4942
HFHSD	Research Diets, NJ	D12331
Liposomal 15-Keto-PGE ₂	Taiwan Liposome Company, Taiwan	Lot #0418
Critical commercial assays		
Nuclear Extraction kit	Abcam, UK	AB113474
NF- κ B p65 transcription factor assay kit	Abcam, UK	AB133112
Luc-Pair Duo-Luciferase HS Assay Kits	Genecoeppia, AR	GCP-LF006
Q5 Site-Directed Mutagenesis Kit	New England BioLabs, MA	E0554S
Mouse Lipopolysaccharides (LPS) ELISA Kit	Cusabio, TX	CSB-E13066m
Cytokines IL6, TNF-a, IL-1 β , MCP-1	ELISA MAX™ Deluxe, BioLegend, CA	431304, 430904, 432604, 432704

(Continued on next page)

Continued

REAGENT or RESOURCE	SOURCE	IDENTIFIER
Experimental models: Cell lines		
RAW264.7	Bioresource Collection and Research Center, Taiwan	60001
HEK293T	Bioresource Collection and Research Center, Taiwan	60019
Experimental models: Organisms/strains		
C57BL/6JNarl	NARLabs, National Laboratory Animal Center, Taiwan	RMRC11005
Oligonucleotides		
Primer pairs, see in Figure S1	This manuscript	N/A
Mutagenic primer, see in STAR Methods	This manuscript	N/A
Recombinant DNA		
IgK-Luc	Dr. Li-Chung Hsu, National Taiwan University	N/A
Renilla luciferase reporter plasmid (pRL-TK)	Promega, WI	E2241
NF- κ B1 (p105/p50)	Origene, MD	MR226792
RelA (p65)	Origene, MD	MR227671
Software and algorithms		
Mascot Daemon	Matrix Science, MA	https://www.matrixscience.com/daemon.html
CellSens Standard 1.14 software	Olympus, Germany	https://www.olympus-lifescience.com/en/software/cellsens/
Image J	NIH	https://ImageJ.nih.gov/
Prism 9	GraphPad, San Diego, CA	https://www.graphpad.com/
Other		
anti-FLAG® M2 Magnetic Beads	Sigma-Aldrich, MO)	M8823
Dynabeads Protein A	Invitrogen	10002D

RESOURCE AVAILABILITY**Lead contact**

Further information and requests for resources and reagents should be directed to and will be fulfilled by the lead contact, Lee-Ming, Chuang (leeming@ntu.edu.tw).

Materials availability

The Cys-15-keto-PGE2 antibody generated in this manuscript will be made available upon request.

Data and code availability

- All data reported in this paper will be shared by the [lead contact](#) upon request.
- This paper does not report original code.
- Any additional information required to reanalyze the data reported in this paper is available from the [lead contact](#) upon request.

EXPERIMENTAL MODEL AND SUBJECT DETAILS**Mouse model of obesity and the formulation of 15-keto-PGE2 for injection**

All animal experiments were approved by the Institutional Animal Care and Use Committee of the Medical College (IACUC) of National Taiwan University [approval number: 20200097]. The mice were housed at 23°C and 12/12 hr light/dark (7 AM-7 PM) cycle in the animal centers of the College of Medicine of National Taiwan University, which is accredited by the Association for Assessment and Accreditation of Laboratory Animal Care International (AAALAC). Eight-week-old C57BL/6J male mice were fed a HFHSD (Research Diets, NJ) for 3 months before the intraperitoneal injection of 15-keto-PGE2, which was dissolved in liposome (20 μ L/g/day) (Taiwan Liposome Company, Taiwan). For

prolonged treatment, C57BL/6J male mice were intraperitoneal injection of 15-keto-PGE2 (10 mg/kg/day) for 6 weeks after feeding on a HFHSD for 10 months, starting at eight weeks of age.

METHOD DETAILS

Cell culture and reagents

The mouse RAW264.7 cells were a gift from Dr. Chia-Li Yu at the Institute of Molecular Medicine of the National Taiwan University College of Medicine. RAW264.7 cells were cultured in RPMI 1640 medium with 10% heat-inactivated fetal bovine serum, L-glutamine, and antibiotics (penicillin, streptomycin, and amphotericin B) (Gibco, CA). HEK293T cells were a gift of Dr. Ya-Wen Liu at the Institute of Molecular Medicine of the National Taiwan University. HEK293T cells were cultured in DMEM medium with 10% fetal bovine serum, L-glutamine, and antibiotics. 15-keto-PGE2 (Cayman, MI) and Lipopolysaccharide, *E. coli* O111: B4 (LPS) (Millipore, MA) were purchased.

RNA Extraction and quantitative PCR

RNA was isolated from cells or tissues using Rezol (PROtech technologies, Taiwan) and was reversely transcribed to cDNA using Maxima H minus Reverse Transcriptase (Thermo Scientific, MA). The mRNA levels were measured by quantitative PCR (qPCR) of cDNA using the Luminaris Color HiGreen qPCR Master Mix (Thermo Scientific) and qPCR amplification was carried out using the LightCycler 2.0 Instrument and the results were analyzed with LightCycler software 4.05 (Roche, Switzerland). The mRNA levels were normalized to cyclophilin expression levels. The primer sequences were listed in [Table S1](#), and the $2^{-\Delta\Delta CT}$ relative quantification method was employed to calculate the fold of change.

Western Blot analysis

Whole-cell lysates were prepared with a RIPA lysis buffer (Millipore) with the addition of protease and phosphatase inhibitors (Roche, Switzerland). Equivalent amounts of protein were separated sodium dodecyl sulfate polyacrylamide gel electrophoresis (SDS-PAGE) and transferred to polyvinylidene fluoride (PVDF) microporous membrane (GE Healthcare Life Sciences, Germany). Membranes were blocked with 3% BSA in PBS containing 0.1% Tween-20. Primary antibodies used for immunoblotting are shown in [key resources table](#). Secondary antibodies were conjugated to horseradish peroxidase (Genetex, CA), and peroxidase activity was visualized using the Luminata Crescendo Western HRP substrate (Millipore). Signals were detected using ImageQuant LAS 4000 (GE Healthcare Life Sciences).

Generation of monoclonal antibodies against 15-keto-PGE2 conjugated to cysteine

Briefly, Balb/c mice were immunized with 15-keto-PGE2-cysteine-ovomucoid (OVO) (100 μ g/mouse) via subcutaneous injection three times at a two-week interval. 10 μ g of 15-keto-PGE2-cysteine-OVO was injected via the tail vein of mice 3 days prior to spleen harvest. Spleen cells were used with the mouse myeloma cell line FO to generate hybridomas using PEG 1500 (Roche, Switzerland). Hybridomas were selected in complete Dulbecco's modified Eagle's medium (DMEM) containing hypoxanthine-aminopterin-thymidine (Thermo Scientific) and UltraCruz Hybridoma Cloning Supplement (Santa Cruz, TX). Positive hybridomas were then cloned and antibody isotypes were determined using a Rapid ELISA mouse mAb Isotyping Kit (Thermo Scientific). Monoclonal antibodies were purified from the culture supernatant of hybridoma cells. The specificity of the generated antibodies were confirmed as demonstrated in [Figure S1](#).

Nuclear-cytoplasmic fractionation

RAW264.7 cells were seeded in 10-cm plates overnight and treated with 15-keto-PGE2 for 2 h, followed by LPS stimulation. After harvesting the cells, nuclear-cytoplasmic fractionation was conducted using the Nuclear Extraction kit (Abcam, UK) according to the manufacturer's instructions.

Transwell migration assay

The transwell migration assay utilized 24-transwell inserts with 8- μ m pore-size membranes (Corning Costar, USA). After pre-treated with either DMSO or 30 μ M 15-keto-PGE2 for 24 hours, 3×10^5 RAW264.7 cells were seeded into the upper chamber using 100 μ l of RPMI medium containing 1% FBS. The lower chamber was filled with 600 μ l of complete medium containing 1 μ g/ml LPS. Following a 24-hour incubation period, non-migrating cells on the upper surface of the insert were gently removed by scraping with a cotton swab. The cells on the lower side were fixed with cold methanol for 15 minutes and stained with crystal violet. Migrated cells were observed using a microscope. For quantification, four images were captured for each membrane using an inverted microscope (Leica, Germany), and ImageJ software was employed for analysis.

NF- κ B p65 transcription factor assays

RAW264.7 cells were harvested after treatment, and nuclear lysates were extracted using the Nuclear Extraction kit (Abcam). The nuclear fraction was used for NF- κ B p65 transcription factor assays according to the recommended experimental protocol (Abcam).

Luciferase reporter assay

RAW264.7 cells were seeded in 12-well plates for 16 h before transfection for the luciferase reporter assay. The reporter construct for NF- κ B activation IgK-Luc, a generous gift from Dr. Li-Chung Hsu's lab at the Institute of Molecular Medicine of the National Taiwan University College of Medicine, was co-transfected into RAW264.7 cells with an internal control of Renilla luciferase reporter plasmid (pRL-TK) (Promega, WI) for 24 h. The cells were then treated with indicated concentration of LPS for indicated time before harvested to determine the luciferase activity. All transfections were performed with TurboFect Transfection Reagents (Thermo Scientific) and luminescence was determined using the Luc-Pair Duo-Luciferase HS Assay Kits (Genecoeppia, AR) according to the manufacturer's instructions.

Plasmid mutagenesis

The mutagenic primers of p65 C120A and NF- κ B1 C59A were designed by the web-based QuickChange Primer Design Program: (5'-ggggatccaggctgtgaagaagcg-3' and 5'-aggttctggaagctatgg-3') and (5'-ggggatccaggctgtgaagaagcg-3' and 5'-aggttctggaagctatgg-3'). The point mutation was generated using the Q5 Site-Directed Mutagenesis Kit (New England BioLabs, MA) according to the manufacturer's instructions.

Immunoprecipitation and proteomic analysis

HEK293T cells, a generous gift from Dr. Ya-Wen Liu at the Institute of Molecular Medicine of the National Taiwan University College of Medicine, were transfected with mouse p105/p50 and p65 plasmids with FLAG-tag (Origene, MD). After 24 h, cells were treated with DMSO or 30 μ M 15-keto-PGE2 for 24 h and collected with lysis buffer (50 mM Tris HCl, pH7.4, with 150 mM NaCl, 1 mM EDTA, and 1% Triton X-100). FLAG-p105/p50 and p65 were immunoprecipitated using anti-FLAG[®] M2 Magnetic Beads (Sigma-Aldrich, MO) according to the manufacturer's instructions. The eluted proteins were separated by SDS-PAGE, followed by Western blot analysis. SDS-PAGE was then stained with Coomassie blue and SYPRO-Ruby staining methods (Sigma-Aldrich), and the bands of interest were excised for in-gel digestion and cleaned via the C18 Zip-Tip method (Millipore).

Shotgun proteomic identifications were performed as previously described.⁴⁹ NanoLC-nanoESI-tandem mass spectrometry analysis was performed using the nanoAcquity system (Waters, MA) connected with the LTQ Orbitrap Velos hybrid mass spectrometer (Thermo Electron, MA) and a PicoView nanospray interface (New Objective, MA). Peptide mixtures were loaded onto a 75 μ m ID, 25 cm length C18-BEH column (Waters, MA) packed with 1.7 μ m particles with a pore of 130 Å. Peptide mixture were separated using a segmented gradient in 60 min from 5% to 40% of solvent B (acetonitrile with 0.1% formic acid) at a flow rate of 300 nl/min at 35°C. Solvent A was 0.1% formic acid in water. Survey full scan MS spectra was acquired in the Orbitrap (m/z 350-1600) with the resolution set to 60K at m/z 400 and automatic gain control target at 5x10⁵ ions. The 10 most intense ions were sequentially isolated for higher-energy C-trap dissociation tandem mass spectrometry fragmentation and detection, with previously selected ions dynamically excluded for 60 s. For tandem mass spectrometry we used a resolution of 7500, an isolation window of 2 m/z, and a target value of 5x10⁴ ions, with maximum accumulation times of 100 ms. Fragmentation was performed with a normalized collision energy of 35% and an activation time of 0.1 ms. Ions with single and unrecognized charge states were excluded. Mascot Daemon (Matrix Science, MA) was used for protein identification and modification.

Measurement of metabolic parameters

Plasma glucose, ALT and AST levels were analyzed using the Cobas C111 analyzer (Roche, Switzerland). Plasma LPS (Cusabio, TX) and insulin (Mercodia, Sweden) were detected using an ELISA kit according to the manufacturer's instructions. Cytokines were measured using ELISA (ELISA MAX[™] Deluxe, BioLegend, CA) or LEGENDplex[™] Multiplex Assays (BioLegend). Fasting glucose level was measured with a glucometer (ACCU-CHECK Performa, Roche) after fasting for 6 h.

Immunohistochemical (IHC) staining

IHC stain was performed on formalin-fixed and paraffin-embedded tissue sections, which were deparaffinized. Antigen retrieval was then conducted at pH 9.0 using the Epitope Retrieval 2 solution (Leica Microsystems, Germany) for 20 minutes at 100°C. The primary antibodies used were F4/80 (Abcam) (1:200) for 30 minutes. Slides were then stained using the Leica Microsystems BOND-MAX autostainer. Post-primary IgG linker reagent localized mouse antibody for 8 minutes. Poly-HRP IgG reagent localized rabbit antibody for 8 minutes. Staining was developed with the substrate chromogen, DAB, for 10 minutes and were counterstained with modified Mayer's hematoxylin for 5 minutes. Images were captured using an Olympus BX51 microscope combined with an Olympus DP72 camera and CellSens Standard 1.14 software (Olympus, Germany).

Liver histopathology

Fresh mouse liver was fixed in 4% paraformaldehyde, paraffin-embedded, sectioned in 4- μ m thickness, and then stained in hematoxylin and eosin (H&E). Stained livers were examined and scored with the NAFLD activity score (NAS) according to the criteria set by Kleiner et al.⁵⁰ Briefly, the score is classified into steatosis (0–3), lobular inflammation (0–2), and hepatocellular ballooning (0–2). If the NAS score of a liver specimen is \geq 5, the specimen is defined as NASH.

Oil Red O staining

Liver tissues were frozen in optimal cutting temperature (OCT) compound and sliced at 5- μ m thickness. The sections were mounted on drying slides and fixed with 10% formalin for 2 h. After fixation, the slides were stained with a 0.5% Oil-Red-O solution (Sigma-Aldrich, MO) for 20 min and then counterstained with hematoxylin (DAKO, CA). Lipid droplet deposition was observed under an optical microscope (Olympus, BX51, Japan).

QUANTIFICATION AND STATISTICAL ANALYSIS

Results were performed with GraphPad Prism version 9.0 (GraphPad Software Inc., San Diego, CA, USA). The results were analyzed using a two-tailed Student's t-test and expressed as mean \pm standard error mean (SEM). Cochran–Armitage trend test was used to calculate p-for-trend among ordinal groups. A two-sided p-value < 0.05 was considered as statistically significant.